

## Magnetic Properties and Crystal Structure of a One-Dimensional Phase of Tetrakis( $\mu_2$ -benzoato-*O,O'*)-bis(dimethyl sulfoxide)dicopper(II)

Yasmi Reyes-Ortega,<sup>\*,†</sup> José L. Alcántara-Flores,<sup>†</sup> María C. Hernández-Galindo,<sup>†</sup> Daniel Ramírez-Rosales,<sup>‡</sup> Sylvain Bernès,<sup>†</sup> Juan C. Ramírez-García,<sup>§</sup> Rafael Zamorano-Ulloa,<sup>‡</sup> and Roberto Escudero<sup>⊥</sup>

Contribution from the Centro de Química, ICUAP. C. U. Puebla, Pue. 72570, México, Departamento de Física, ESFM, IPN, México, D.F. 07738, México, Facultad de Ciencias Químicas. C. U. Puebla, Pue. 72570, México, and Instituto de Investigaciones en Materiales, UNAM. A. Postal 70-360. México, D.F. 04510 México

Received August 15, 2005; E-mail: yreyes@siu.buap.mx.

**Abstract:** A new crystalline polymorphic phase of tetrakis( $\mu_2$ -benzoato-*O,O'*)-bis(dimethyl sulfoxide)dicopper(II) was obtained by direct synthesis, in space group  $P2_1/n$ . The copper coordination is in a slightly distorted square pyramidal geometry with an intramolecular Cu...Cu distance of 2.6494(8) Å. The Cu–O distances of the two copper in a dimer are different, giving different chemical environments for each Cu ion. The crystal structure is built up of well-separated stacking columns oriented along the *b*-axis, with units uniformly spaced, producing a one-dimensional (1-D) zigzag chain through Cu(II)–S...S–Cu(II) interdimer interactions [S...S separation: 3.975(2) Å]. Magnetization measurements in the range 2–300 K indicate two magnetic orderings, at low temperature ( $T < 10$  K) a weak ferromagnetic ordering is observed, and above this temperature an antiferromagnetic behavior takes place. ESR spectra at 300 and 77 K of a polycrystalline sample show the characteristic signal of zero-field with  $D = 0.354$  cm<sup>-1</sup>, consistent with a ferromagnetic Cu...Cu exchange interaction at low temperature.

### 1. Introduction

Structural characteristics of binuclear copper complexes, such as dimeric copper(II) species, have been reported in the past. They proved difficult to obtain, particularly when unpaired electrons should be located in orbitals with orthogonal interactions.<sup>1–8</sup> The magnetic behavior in these compounds is strongly related to the Cu...Cu distance, bond angles, neighboring atoms, local symmetry, and bridging atoms.<sup>1–8</sup> Heintz et al. found that the coupling leading to a parallel alignment of spins is so weak that it hardly could persist at room temperature;<sup>9</sup> this implies that the synthesis of materials with ferro-

magnetic ordering is a difficult task from the chemical point of view. From the physical side, it is important to mention that one-dimensional solids also present distortions in the crystalline state, due to effects related to Peierls transitions, as spin density waves or charge density waves.<sup>10–15</sup> These processes in some compounds may be important if the magnetic ordering is related to a distortion due to a spin density wave.

In the present work we report studies on the synthesis, crystal structure, and magnetic characteristics of a new polymorph of a well-known material, namely tetrakis( $\mu_2$ -benzoato-*O,O'*)-bis(dimethyl sulfoxide)dicopper(II), **1a**. The most interesting aspect is that this phase exhibits a magnetic transition related to ordering at low and at high temperatures. We propose a mechanism for the magnetic ordering, based on magnetic exchange of the copper ions bridged by sulfur atoms of symmetry-related molecules, or by an antiparallel spins align-

<sup>†</sup> Centro de Química, ICUAP.

<sup>‡</sup> Departamento de Física, ESFM.

<sup>§</sup> Facultad de Ciencias Químicas.

<sup>⊥</sup> Instituto de Investigaciones en Materiales, UNAM.

- (1) Charlot, M.-F.; Kahn, O.; Chaillet, M.; Larrieu, C. *J. Am. Chem. Soc.* **1986**, *108*, 2574–2581.
- (2) Melník, M.; Dunaj-Jurčo, M.; Handlovič, M. *Inorg. Chim. Acta* **1984**, *86*, 185–190.
- (3) Tuna, F.; Patron, L.; Journaux, Y.; Andruh, M.; Plass, W.; Trombe, J.-C. *J. Chem. Soc., Dalton Trans.* **1999**, 539–546.
- (4) Fernández, I.; Ruiz, R.; Faus, J.; Julve, M.; Lloret, F.; Cano, J.; Ottenwælder, X.; Journaux, Y.; Muñoz, M. C. *Angew. Chem., Int. Ed.* **2001**, *40*, 3039–3042.
- (5) Koner, S.; Saha, S.; Mallah, T.; Okamoto, K.-I. *Inorg. Chem.* **2004**, *43*, 840–842.
- (6) Kahn, O.; Sikorav, S.; Gouteron, J.; Jeannin, S.; Jeannin, Y. *Inorg. Chem.* **1983**, *22*, 2877–2883.
- (7) Comarmond, J.; Plumeré, P.; Lehn, J.-M.; Agnus, Y.; Louis, R.; Weiss, R.; Kahn, O.; Morgenstern-Badarau, I. *J. Am. Chem. Soc.* **1982**, *104*, 6330–6340.
- (8) Willett, R. D.; Breneman, G. L. *Inorg. Chem.* **1983**, *22*, 326–329.

- (9) Heintz, R. A.; Koetzle, T. F.; Ostrander, R. L.; Rheingold, A. L.; Theopold, K. H.; Wu, P. *Nature* **1995**, *378*, 359–362.
- (10) Allan, M. L.; Coomber, A. T.; Marsden, I. R.; Martens, J. H. F.; Friend, R. H.; Charlton, A.; Underhill, A. E. *Synth. Met.* **1993**, *56*, 3317–3322.
- (11) Woodard, B.; Willett, R. D.; Haddad, S.; Twamley, B.; Gomez-Garcia, C. J.; Coronado, E. *Inorg. Chem.* **2004**, *43*, 1822–1824.
- (12) Ren, X.; Meng, Q.; Song, Y.; Hu, C.; Lu, C.; Chen, X.; Xue, Z. *Inorg. Chem.* **2002**, *41*, 5931–5933.
- (13) Gadet, V.; Mallah, T.; Castro, I.; Verdager, M.; Veillet, P. *J. Am. Chem. Soc.* **1992**, *114*, 9213–9214.
- (14) Bray, J. W.; Hart, H. R., Jr.; Interrante, L. V.; Jacobs, I. S.; Kasper, J. S.; Watkins, G. D.; Wee, S. H.; Bonner, J. C. *Phys. Rev. Lett.* **1975**, *35*, 744–747.
- (15) Tandon, S. S.; Chen, L.; Thompson, L. K.; Bridson, J. N. *Inorg. Chem.* **1994**, *33*, 490–497.

ment of the two copper(II)-homonuclear units through the intramolecular eight oxygen bridging atoms belonging to the four benzoato ligands.

## 2. Experimental Methods

**2.1.** Electronic spectra were measured with a Shimadzu UV-3100S spectrophotometer on ca.  $10^{-4}$  M chloroform solutions at 298 K ( $\lambda = 200\text{--}2200$  nm). A Nicolet Magna-IR 750 spectrophotometer was employed to monitor the infrared spectra, using KBr and polyethylene pellets. ESR spectra at X-band frequency were obtained with a JEOL JES-RES 3X spectrometer, from 300 to 77 K, on polycrystalline powder samples. Magnetic measurements were performed in gelatin capsule using a Quantum Design magnetometer. The calculated Pascal<sup>16</sup> constant for compound **1a** is about  $264 \times 10^{-6}$  emu and was not taken into account, owing to its small value as compared with the measured data. Measurements were performed in small magnetic fields, from 20 to 180 G, and in the range 2–300 K, in zero field-cooling (ZFC) and field-cooling (FC) modes.

**2.2.** The synthesis of **1a** was carried out using the direct synthesis method.<sup>17</sup> Equimolar amounts (0.3143 mmol) of copper(0), (–)-sparteine (sp), benzoyl bromide, and dimethyl sulfoxide (DMSO) (0.85 mL) were placed in a flask, and the mixture was stirred at 70 °C for 24 h. The mixture was then filtered at 70 °C and the resulting solution cooled to room temperature, allowing the separation of **1a** as dark-green crystals suitable for X-ray crystallography (yield: 5%), **1b**, which was identified as the phase previously reported for the same compound (yield: 64%),<sup>2</sup> and other products identified as:  $[(\text{Br})(\text{PhCO}_2)(\text{sp})]\text{Cu}(\text{II})$ ,<sup>18</sup>  $[\text{Br}_2(\text{sp})]\text{Cu}(\text{II})$ ,<sup>19</sup>  $[\text{Br}_2(\text{DMSO})_2]\text{Cu}(\text{II})$ ,<sup>20</sup> and  $[(\text{PhCO}_2)_2(\text{sp})]\text{Cu}(\text{II})$ .<sup>21</sup> **1a**: mp 268–270 °C dec UV–vis /CHCl<sub>3</sub>  $\lambda_{\text{max}}/\epsilon$  (nm/M<sup>-1</sup> cm<sup>-1</sup>): 273/2479, 667/731; IR/KBr, PET  $\nu$  (cm<sup>-1</sup>):  $\nu$  (COO) 1633 *st. asymm.*,  $\nu$  (COO) 1406 *st. symm.*,  $\nu$  (DMSO) 1024,  $\nu$  (Cu–O) 495; ESR (powdered sample) at 300 and 77 K:  $g_1 = 16.966$ ,  $g_2 = 3.508$ ,  $g_3 = 2.287$ ,  $g_4 = 1.953$ ,  $g_5 = 1.417$ ,  $g_6 = 1.385$ .

**2.3.** X-ray diffraction data were collected at 296 K on a P4 diffractometer using Mo K $\alpha$  radiation ( $\lambda = 0.71073$  Å) and following standard procedures.<sup>22</sup> Relevant crystallographic data are listed in Table 1. Data were collected at 0.84 Å resolution and corrected for absorption effects on the basis of 20  $\psi$ -scans (transmission factors in the range 0.673–0.774). The structure was solved and refined using routine methods.<sup>23,24</sup> H atoms were placed in idealized positions and constrained to ride on their carrier C atoms. In the last difference map, two high residuals are observed close to S atoms of DMSO molecules. Attempts

**Table 1.** Crystallographic Data of **1a**

|   |  |
|---|--|
| formula   | C <sub>32</sub> H <sub>32</sub> Cu <sub>2</sub> O <sub>10</sub> S <sub>2</sub> |
| fw  | 767.78   |
| crystal system  | monoclinic   |
| space group   | <i>P</i> 2 <sub>1</sub> / <i>n</i>   |
| <i>Z</i> , <i>Z'</i>  | 4, 1   |
| <i>a</i> , Å  | 12.0407(9)   |
| <i>b</i> , Å  | 17.0916(13)  |
| <i>c</i> , Å  | 17.2680(15)  |
| $\beta$ , deg   | 103.062(6)   |
| <i>V</i> , Å <sup>3</sup>                                   | 3461.7(5)  |
| $\rho_{\text{calc}}$ , g.cm <sup>-3</sup>                   | 1.473  |
| <i>m</i> , mm <sup>-1</sup>                                 | 1.402  |
| <i>R</i> <sub>1</sub> , <i>wR</i> <sub>2</sub> <sup>a</sup> | 0.0540, 0.0840   |
| GOF <sup>a</sup>  | 1.016  |

<sup>a</sup>

$$R_1 = \frac{\sum ||F_o| - |F_c||}{\sum |F_o|}, wR_2 = \sqrt{\frac{\sum w(F_o^2 - F_c^2)^2}{\sum w(F_o^2)^2}}, S = \sqrt{\frac{\sum w(F_o^2 - F_c^2)^2}{m - n}}$$

to model S atoms with disordered sites, although slightly improving *R* indices, were unsatisfactory, since they produced prolate thermal ellipsoids and did not converge to a sensible geometry for the minor parts of disordered sites. Highest residuals probably reflect thermal motions for S atoms rather than actual disorders.

## 3. Results and Discussion

**3.1. Synthesis.** The direct synthesis method, based on the use of zerovalent metals as starting materials, provides a suitable environment for the synthesis of different complexes of copper(II) as many ligands are present in the reaction medium. The control of the reaction conditions (temperature, reaction time, and solvent) allows increasing the yield of the complex of interest without residual salts. The absence of residual salts greatly favors the formation of pure phases, which may be easily separated from the reaction medium.<sup>25</sup> In the present work, this methodology was essential for the isolation of two polymorphs for the complex  $[(\text{PhCO}_2)_4(\text{DMSO})_2]\text{Cu}_2$ , **1a** and **1b**, one of which, **1a**, is obtained with 5% yield.

**3.2. Solid-State Structure.** The asymmetric unit of **1a** consists of one binuclear Cu(II) complex in general position, including four bridging benzoato ligands and two coordinated DMSO molecules (Figure 1). The geometry around each Cu(II) ion in the dimer unit may be described by a slightly distorted square pyramid, consistent with small geometric  $\tau$  parameters: <sup>26</sup> 0.026 Å for Cu1 and 0.100 Å for Cu2. Four O atoms of the four benzoato moieties conform the square base, with Cu–O bond lengths spanning the small range 1.947(3)–1.984(3) Å (Table 2). DMSO molecules are axially coordinated to the metallic centers through their O atoms, at expected distances, 2.137(3) and 2.157(3) Å. The bridging networks Cu–O–C–O–Cu are planar and give a Cu $\cdots$ Cu separation of 2.6494(8) Å. This is shorter than some distances previously reported<sup>1,8,15,27–29</sup> but comparable to the mean value of 2.661 Å, computed from

(16) O'Connor, C. J. In *Progress in Inorganic Chemistry*; Lippard, S. J., Ed.; Wiley: EUA, 1982; Vol. 29, p 203.

(17) Gutiérrez, R.; Yáñez, J.; Vázquez, R. A.; Reyes, Y.; Toscano, R. A.; Martínez, M.; Álvarez, C. *J. Coord. Chem.* **2001**, *54*, 313–321.

(18) Reyes-Ortega, Y.; Alcántara-Flores, J.-L.; Hernández-Galindo, M. C.; Gutiérrez-Pérez, R.; Ramírez-Rosales, D.; Bernès, S.; Durán-Hernández, A.; Zamorano-Ulloa, R. *J. Mol. Struct.* Manuscript submitted

(19) Alcántara-Flores, J. L.; Ramírez-Rosales, D.; Bernès, S.; Pérez-Ramírez (Bokhimi), J. G.; Durán-Hernández, A.; Gutiérrez-Pérez, R.; Zamorano-Ulloa, R.; Reyes-Ortega, Y. *J. Mol. Struct.* **2004**, *693*, 125–131.

(20) Willett, R. D.; Jardine, F. H.; Roberts, S. A. *Inorg. Chim. Acta* **1977**, *25*, 97–101.

(21) Reyes-Ortega, Y.; Alcántara-Flores, J.-L.; Hernández-Galindo, M. del C.; Gutiérrez-Pérez, R.; Ramírez-Rosales, D.; Bernès, S.; Cabrera-Vivas, B. M.; Durán-Hernández, A.; Zamorano-Ulloa, R. Manuscript to be submitted.

(22) *XSCAnS Users Manual*, release 2.21; Siemens Analytical X-ray Instruments Inc.: Madison, WI, 1996.

(23) Sheldrick, G. M. *SHELXTL-Plus*, release 5.10; Siemens Analytical X-ray Instruments Inc.: Madison, WI, 1998.

(24) Sheldrick, G. M. *SHELX 97-2, Users Manual*; University of Göttingen: Germany 1997.

(25) Sikorav, S.; Bkouche-Waksman, I.; Kahn, O. *Inorg. Chem.* **1984**, *23*, 490–495.

(26) Addison, A. W.; Nageswara Rao, T.; Reedijk, J.; van Rijn, J.; Verschoor, G. C. *J. Chem. Soc., Dalton Trans.* **1984**, 1349–1356.

(27) McKee, V.; Dagdigian, J. V.; Bau, R.; Reed, C. A. *J. Am. Chem. Soc.* **1981**, *103*, 7000–7001.

(28) Rodríguez-Martín, Y.; Ruiz-Pérez, C.; Sanchiz, J.; Lloret, F.; Julve, M. *Inorg. Chim. Acta* **2001**, *318*, 159–165.

(29) Mallah, T.; Boillot, M.-L.; Kahn, O.; Gouteron, J.; Jeannin, S.; Jeannin, Y. *Inorg. Chem.* **1986**, *25*, 3058–3065.

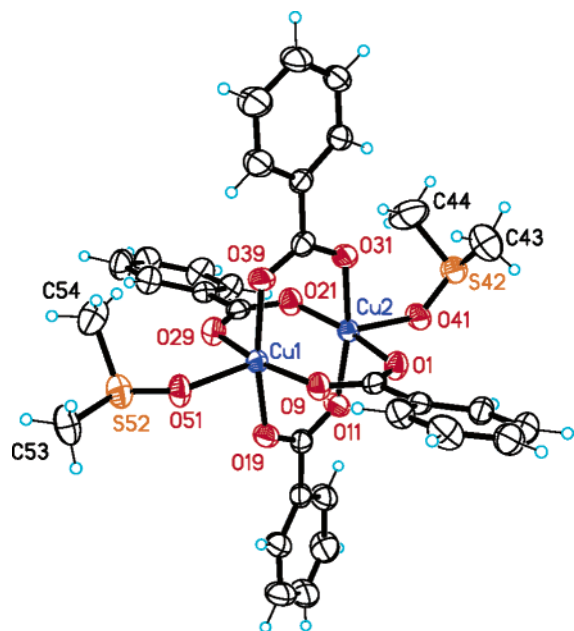


**Figure 1.** Molecular structure and numbering scheme for the binuclear unit complex in **1a**. Thermal ellipsoids for non-H atoms are drawn at the 30% probability level.

**Table 2.** Selected Bond Distances and Angles for **1a** (Å,  $\theta$  deg)

| Bond Distances  |           |                 |            |
|-----------------|-----------|-----------------|------------|
| Cu1—O9          | 1.971(3)  | Cu1—O19         | 1.972(3)   |
| Cu1—O29         | 1.985(3)  | Cu1—O39         | 1.962(3)   |
| Cu2—O1          | 1.964(3)  | Cu2—O11         | 1.949(3)   |
| Cu2—O21         | 1.947(3)  | Cu2—O31         | 1.984(3)   |
| Cu2—O41         | 2.157(3)  | Cu1—O51         | 2.137(3)   |
| Bond Angles     |           |                 |            |
| O9—Cu1—O19      | 90.45(15) | O9—Cu1—O29      | 167.05(14) |
| O9—Cu1—O39      | 89.16(15) | O9—Cu1—O51      | 96.32(13)  |
| O19—Cu1—O29     | 89.02(15) | O19—Cu1—O39     | 167.54(15) |
| O19—Cu1—O51     | 94.25(15) | O29—Cu1—O39     | 88.59(15)  |
| O29—Cu1—O51     | 96.62(13) | O39—Cu1—O51     | 98.17(15)  |
| O1—Cu2—O11      | 90.75(16) | O1—Cu2—O21      | 168.34(14) |
| O1—Cu2—O31      | 89.35(15) | O1—Cu2—O41      | 95.16(14)  |
| O11—Cu2—O21     | 88.36(16) | O11—Cu2—O31     | 167.75(14) |
| O11—Cu2—O41     | 89.70(15) | O21—Cu2—O31     | 89.07(15)  |
| O21—Cu2—O41     | 96.47(15) | O31—Cu2—O41     | 102.49(14) |
| Torsion Angles  |           |                 |            |
| C43—S42—O41—Cu2 | 55.7(5)   | C44—S42—O41—Cu2 | -47.3(5)   |
| C53—S52—O51—Cu1 | 175.7(3)  | C54—S52—O51—Cu1 | -80.0(4)   |

432 entries found in the CSD including a tetrakis( $\mu_2$ -benzoato-*O,O'*)dicopper(II) fragment.

This geometry for the central core of **1a** is very close to that previously described for the polymorph **1b**, crystallizing in space group  $C2/c$ , with a  $\text{Cu}\cdots\text{Cu}$  separation of 2.627(3) Å.<sup>2</sup> However, a comparison of the molecular structures for both polymorphs shows different conformations for one of the two DMSO molecules with respect to the central core; this DMSO molecule is rotated by ca. 180° around the formal  $\sigma$  bond  $\text{Cu}-\text{O}(\text{DMSO})$ . In the case of **1a**, C—S—O—Cu torsion angles describe  $+sc/-sc$  and  $ap/-sc$  conformation for DMSO molecules coordinated to Cu2 and Cu1, respectively (Table 2), while in the case of **1b**, these descriptors show the DMSO molecules to be  $+sc/-sc$  and  $ap/+sc$  ( $sc$  stands for *syn*-clinal or *gauche*, and  $ap$  stands for *anti*-periplanar or *trans*). In other words, DMSO molecules are arranged *cis* with respect to the  $\text{Cu}\cdots\text{Cu}$  line in **1a**, and almost *trans* in **1b**.

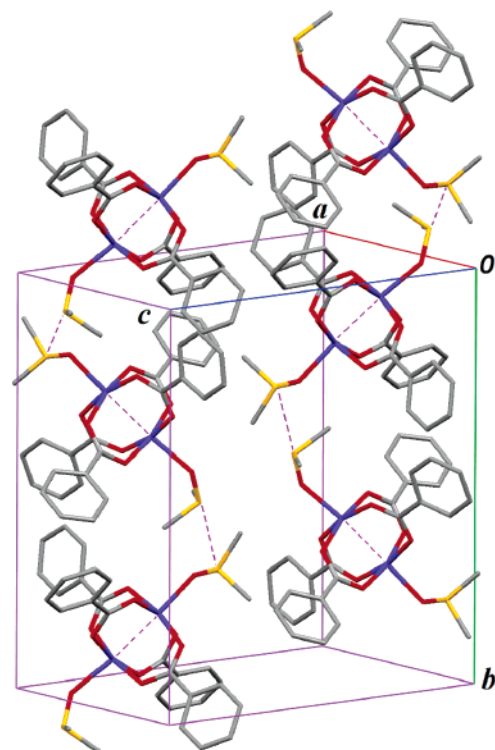


**Figure 2.** View of the infinite 1-D zigzag chains parallel to the crystallographic  $b$ -axis. Dashed lines represent  $\text{Cu}\cdots\text{Cu}$  separations within dimers and intermolecular  $\text{S}\cdots\text{S}$  magnetic interactions generating the supramolecular structure. For the sake of clarity, H atoms have been omitted.

This free rotation for DMSO, along with a symmetry modification, is reflected in essentially different crystal structures for **1a** and **1b**. In the former case, dimer units are joined through  $\text{S}\cdots\text{S}$  contacts and form zigzag chains oriented parallel to the [010] axis. It is worth noting that a single  $\text{S}\cdots\text{S}$  separation is observed in this one-dimensional (1-D) supramolecular structure, characterized by a single distance,  $\text{S}\cdots\text{S}^i = 3.975(2)$  Å [symmetry code: (i)  $3/2 - x, -1/2 + y, 3/2 - z$ ]. In the same way, zigzag chains are built up on a single angle, for instance 54.39°, the angle between consecutive  $\text{Cu}\cdots\text{Cu}$  vectors along the chain (Figure 2). The steric demand of benzoato groups avoid significant contacts between neighboring chains in the crystal, such as hydrogen bonds. **1a** may be thus considered, at least at 296 K, as an actual 1-D system of the type  $\cdots\text{A}-\text{A}-\text{A}\cdots$  where A is the dimer unit. In the case of **1b**, a short  $\text{S}\cdots\text{S}$  contact is also observed between two symmetry-related molecules in the unit cell (3.718 Å). However, the supramolecular character of **1b** is limited to these dimers of dimers, since the conformation of DMSO molecules and intermolecular distances do not allow linking these units to form a polymeric structure. As a result, the crystal structure of **1a** makes this system potentially accessible to a Peierls transition at low temperature, while such a transition is very unlikely to occur for polymorph **1b**.

**3.3. UV–Vis and IR Spectroscopy.** The UV/vis, NIR spectrum shows  $\pi-\pi^*$  transitions at 273 nm with  $\epsilon = 2479$   $\text{M}^{-1} \text{cm}^{-1}$  and at 667 nm with  $\epsilon = 731$   $\text{M}^{-1} \text{cm}^{-1}$ .<sup>30</sup> It is possible to observe the characteristic band assigned to d–d transitions for distorted square-pyramidal copper(II) centers, in agreement with the X-ray structure determination.<sup>2,31</sup> The IR

(30) Du, M.; Guo, Y.-M.; Chen, S.-T.; Bu, X.-H.; Ribas, J. *Inorg. Chim. Acta* **2003**, *346*, 207–214.

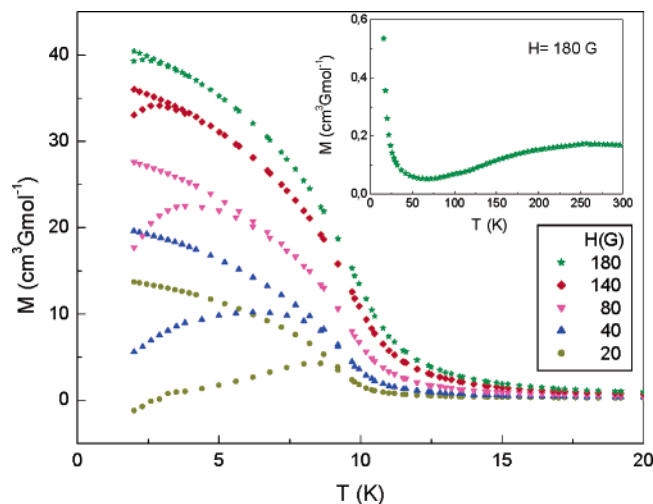


**Figure 3.** Thermal dependence of the magnetization at different magnetic field intensities  $H$ . Note the change of the magnetization from low to high field. At about 80 G the behavior is clearly ferromagnetic. The inset shows  $M$ - $T$  curve measured from low to room temperature at 100 G in the FC mode. It seems that the magnetization is increasing from about 60 K to above, indicating a magnetic ordering persisting at room temperature, with a maximum at ca. 260 K.

spectrum shows the  $\nu_{\text{COO}^-}$  at  $1633\text{ cm}^{-1}$ , and a vibration characteristic of DMSO<sup>2,31,32</sup> at  $1024\text{ cm}^{-1}$ . Far-infrared spectrum shows the characteristic vibration  $\nu_{\text{Cu-O}}$  at  $495\text{ cm}^{-1}$ .<sup>33</sup>

**3.4. Magnetic Measurements.** Magnetization vs temperature ( $M$ - $T$ ) measurements are presented in Figure 3, where  $M$  is the molar magnetization of the binuclear unit in both ZFC and FC measurements. For the sake of clarity, only five  $M$ - $T$  curves at different field strengths are depicted in Figure 3. It should be noted that all the curves present two branches at low temperature; at a given field, the low branch is the ZFC part, whereas the upper branch corresponds to FC measurement. This irreversibility decreases as the magnetic strength increases, and at about 180 G the irreversibility almost disappears. As the magnetic strength is increased, the maximum observed in ZFC is displaced at lower temperatures, approximately in a linear form. At low field, 20 G, the maximum is at about 8 K, and decreases to 2.5 K with a field of about 180 G. This behavior of the magnetization curves clearly indicates a weak ferromagnetism.<sup>11,33</sup> The inset in Figure 3 shows the magnetic ordering at high temperature, starting from about 12 K to above. This behavior may be related to an antiferromagnetic ordering due to uncompensated spin alignment. The maximum on this curve is found at  $T = 260 \pm 6\text{ K}$ , which means that using a Bonner and Fisher fit would result in  $J < 0$ ; the susceptibility passes through a rounded maximum at a temperature  $T_{\text{max}}$  defined by  $kT_{\text{max}}/|J| = 0.641$ , giving a value  $J = -282 \pm 6\text{ cm}^{-1}$ .<sup>34, 35</sup>

To understand more about the magnetic characteristics of **1a**, we studied the  $M$ - $H$  isothermal measurements in the range 1.7–15 K (Figure 4). A magnetization close to saturation is observed

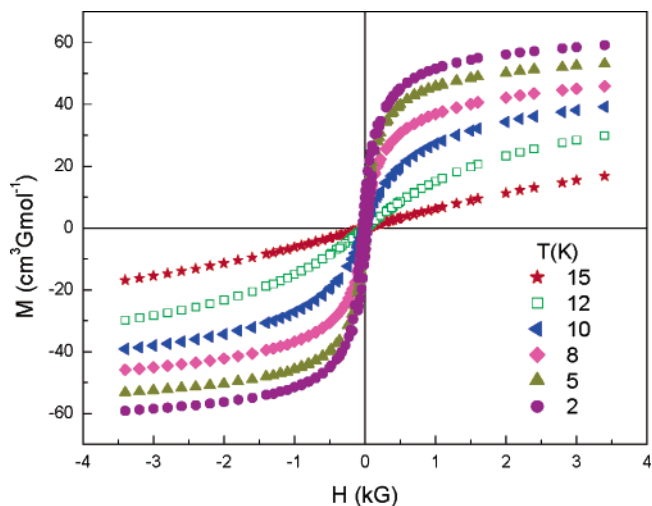


**Figure 4.** Isothermal magnetization measurements  $M$ - $H$  from 2 to 15 K. At 2 K and 3 kG the saturation magnetization value is  $M_s \approx 0.012\text{ mB}$ .

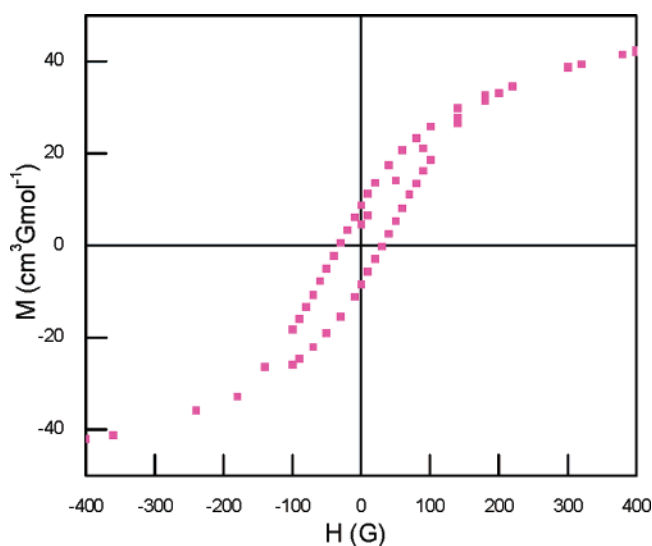


**Figure 5.** Isothermal magnetization  $M$ - $H$  data at 2 K, in the range  $\pm 400\text{ G}$ . Note the coercive field with value of about 72 G.

at 2 K, with measurements performed up to 4000 G. However, as the temperature is increased, the saturation is not longer reached. At 15 K, a small hysteresis is observed in  $M$ - $H$  curves, but this is larger than the hysteresis at 10 and 12 K measurements, indicating an antiferromagnetic behavior due to canted and uncompensated spin alignment.

In Figure 5 for example, we present  $M$ - $H$  data measured at 2 K. The curve shows the coercive field, and in Figure 6 we present those values, extracted from data of Figure 4. Dots represent the experimental values of the coercive field, and the dashed line is a fit to the equation:  $H_C(T) = H_C(0)\{1 - (T/T_C)^{1/2}\}$ , up to about 10 K; above this temperature, the coercive field starts to increase again, and the fit no longer holds. However, the fit gives the following parameters: Curie temperature,  $T_C = 9.0\text{ K}$ ;  $H_C(0) = 60\text{ G}$ . The fit looks adequate, indicating the onset of different uncompensated spin ordering above 10 K. At  $T > 10\text{ K}$  the signature of the spin-uncompensated antiferromagnetism is observed, showing a rising small coercive field.

Data of  $M$ - $H$  measured at 2 K show that the magnetization increases rapidly up to 1100 G, and reach saturation at  $M_s \approx$

- (31) Alcántara-Flores, J. L.; Vázquez-Bravo, J. J.; Gutiérrez-Pérez, R.; Ramírez-Rosales, D.; Bernès, S.; Ramírez Bokhimi, J. G.; Zamorano-Ulloa, R.; Reyes-Ortega, Y. *J. Mol. Struct.* **2003**, *657*, 137–143.
- (32) Nakamoto, K. *Infrared, Raman Spectra of Inorganic and Coordination Compounds*, 4th ed.; Wiley: New York, 1986.
- (33) Li, D.; Zheng, L.; Zhang, Y.; Huang, J.; Gao, S.; Tang, W. *Inorg. Chem.* **2003**, *42*, 6123–6129.
- (34) Boillot, M.-L.; Journaux, Y.; Bencini, A.; Gatteschi, D.; Kahn, O. *Inorg. Chem.* **1985**, *24*, 263–267.
- (35) Acevedo-Chávez, R.; Costas, M. E.; Escudero, R. *J. Solid State Chem.* **1997**, *132*, 24–32.

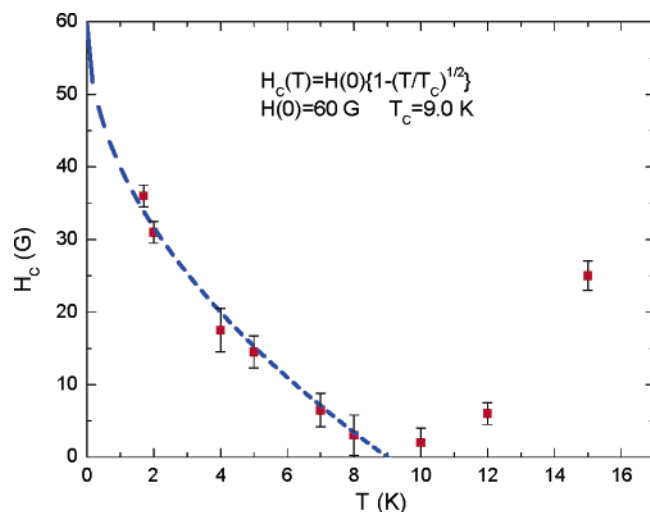


**Figure 6.** Coercive field vs temperature. The fit to the equation  $H_c(T) = H_c(0)\{1 - (T/T_c)^{1/2}\}$  gives values:  $H_c(0) = 60$  G, and  $T_c = 9.0$  K. Above 10 K the coercive field increases, indicating an uncompensated antiferromagnetic behavior. The bars indicate the uncertainty of the measurement.

0.012 m<sub>B</sub>, assuming a *g* Landé factor of 2. Using the saturation magnetization equation  $M_s = |Ng\mu_\beta S_{\text{total}}|$ , we estimate  $S_{\text{total}} = 0.006$ .<sup>36,37</sup>

The orbital coupling due to Cu1 ion is mainly of a  $d_{x^2-y^2}$  type, extended along the coordination with  $\pi$  orbitals of the oxygen benzoato atoms. On Cu2 ion, the orbital is mainly a  $d_{xy}$  type orbital, extended along the coordination with the  $\pi$  orbitals of the other oxygen atoms in the same benzoato ligand. Each benzoato group being coordinated to the two copper(II) ions in each dimer unit, the whole structure is distorted and the Cu1–O–C–O–Cu2 plane may be rotated in such a way that magnetic orbitals are located in the *xy*-plane and that both are accidentally orthogonal at low temperature.<sup>24,38</sup> This structure implies that magnetic orbitals of each copper ion,  $d_{x^2-y^2}$  and  $d_{xy}$ , are parallel and rotated by about 45° to one another. The magnetic orbital position is only slightly overlapped, resulting in a weak ferromagnetic ordering. The effect of temperature is an important factor that changes the interaction between orbitals; at room temperature the overlap integral, *S*, is small, but at low temperature the *S* value is close to zero.<sup>7</sup> This value changes because positive zones of the overlap density compensate for the negative zones. Finally, it is important to mention that another possibility for the magnetic interactions is through dimeric unit interaction by means of axially coordinated DMSO molecules.

**3.5. ESR Studies.** The powder X-band ESR spectra of **1a** at 300 and 77 K show four transitions (Figure 7). Spectra are typical of a triplet state which exhibits six features arising from  $-1 \rightarrow 0$  and  $0 \rightarrow +1$  transitions, each with *x*, *y*, and *z* components.<sup>7,39–42</sup> There is a feature at 395.85 G (*g* = 16.966) which corresponds to the zero field split for a triplet state in

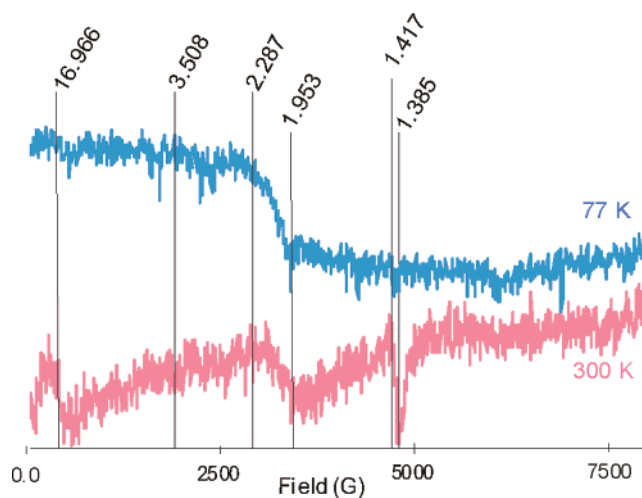


**Figure 7.** ESR spectra at 77 and 300 K of a powdered sample of **1a**.

binuclear copper(II) complexes. Hence, the Cu(II) ions should be ferromagnetically coupled.

The spin Hamiltonian characterizing the triplet ground state, with total spin  $S = 1$  is:  $\mathbf{H} = (\beta H g S) + D[S_z^2 - 1/3 S(S + 1)] + E(S_x^2 - S_y^2)$ , where *D* is the crystal field terms with spin  $S = 1$  and with axial crystal field. The eigen-energies of this subsystem under an axial field,  $D \neq 0$ ,  $E = 0$ ,<sup>33</sup> is adequate to rationalize the experimental ESR signals. From the ESR spectra, *D* is approximately 0.354 cm<sup>-1</sup>. In the  $\Delta M_s = \pm 2$  region, no signals are detected. There is a poorly resolved signal at 2091.99 G (*g* = 3.508). Other clear features are observed at 3300.00 G (*g* = 2.287); at 3375.82 G (*g* = 1.953) two more features are in the region of 4635.20 G (*g* = 1.417) and at 4741.75 G (*g* = 1.385). Attempts for obtaining a more complete interpretation about this magnetically complex system from the ESR spectra were unsuccessful.

#### 4. Conclusions

From these magnetic studies reported here, we conclude that the observed weak ferromagnetic behavior is related to a ferromagnetic exchange interaction via Cu(II)–Cu(II) at low temperatures. This is consistent with the presence of a ground triplet state observed by the zero-field signal in the ESR spectra at 300 and 77 K, although the signals of the ESR spectrum at 77 K are smaller than those at 300 K. It is important to mention that the behavior at low temperatures may also be related to uncompensated antiferromagnetic ordering due to canted spins. In line with results described by Comarmond et al.,<sup>7</sup> in a weak interaction, the two spin levels are thermally populated at room temperature in such a way that  $J_{\text{total}}$  will be the sum of the negative antiferromagnetic  $J_{\text{AF}}$  and positive ferromagnetic  $J_{\text{F}}$  contributions,  $J_{\text{total}} = J_{\text{AF}} + J_{\text{F}}$ , with  $J_{\text{AF}} = -2\Delta S$  and  $J_{\text{F}} = 2C$  (where *S* is the overlap integral between magnetic orbitals and *C* is the two-electron exchange integral). An additional aspect related to the influence of a Peierls distortion in this compound, and which may be related to the observed magnetic effects in this material, is that spin coupling influences the formation of a spin density wave at about 9 K (see Figure 6). Thus, the changes from antiferromagnetic behavior at high temperature to ferromagnetism at low temperature could be related to that distortion. The low value of the saturation magnetization,  $M_s$ ,

(36) Bonner, J. C.; Fisher, M. E. *Phys. Rev. A* **1964**, *135*, 640–658.

(37) Mallah, T.; Thiébaud, S.; Verdaguer, M.; Veillet, P. *Science* **1993**, *262*, 1554–1557.

(38) Ferlay, S.; Mallah, T.; Ouahès, R.; Veillet, P.; Verdaguer, M. *Nature* **1995**, *378*, 701–703.

(39) Kahn, O.; Tola, P.; Galy, J.; Coudanne, H. *J. Am. Chem. Soc.* **1978**, *100*, 3931–3933.

(40) Tirado-Guerra, S.; Cuevas-Garibay, N. A.; Sosa-Torres, M. E.; Zamorano-Ulloa, R. *J. Chem. Soc., Dalton Trans.* **1998**, 2431–2436.

(41) Sugiura, Y. *Inorg. Chem.* **1978**, *17*, 2176–2182.

(42) Marsh, W. E.; Patel, K. C.; Hatfield, W. E.; Hodgson, D. J. *Inorg. Chem.* **1983**, *22*, 511–515.

at 2 K, implies that the Cu(II) electrons have canted spins. At higher fields, a parallel spin alignment would give rise to a higher magnetization value; this assumption explains the  $M-T$  behavior observed when the external field is increased, changing the antiferromagnetic behavior to a ferromagnetic ordering in the 1-D molecular polymer **1a**. In conclusion, **1a** is a molecular solid featuring structural characteristics suitable for the coexistence of both magnetic phases in the bulk material.

**Acknowledgment.** The present work has been supported by Secretaría de Educación Pública and Sub-Secretaría de Educa-

ción Superior and Vicerrectoría de Investigación y Estudios de Posgrado from BUAP, project No. II 163-04/NAT/G.

**Supporting Information Available:** X-ray crystallographic file of **1a** (CIF). This material is available free of charge via the Internet at <http://pubs.acs.org>. The CIF file is also available on application to the Cambridge Data Centre, 12 Union Road, Cambridge CB21EZ, U.K. (Fax: (+44) 1223-336-033. E-mail: [deposit@ccdc.cam.ac.uk](mailto:deposit@ccdc.cam.ac.uk)).

JA055316R